NASA Technical Paper 1018

Cold-Air Performance of a 12.766-Centimeter-Tip-Diameter Axial-Flow Cooled Turbine

II - Effect of Air Ejection on Turbine Performance

Jeffrey E. Haas and Milton G. Kofskey

AUGUST 1977

NASA Technical Paper 1018

Cold-Air Performance of a 12.766-Centimeter-Tip-Diameter Axial-Flow Cooled Turbine

II - Effect of Air Ejection on Turbine Performance

Jeffrey E. Haas and Milton G. Kofskey

Lewis Research Center
and
Lewis Directorate,
U.S. Army Air Mobility R&D Laboratory
Cleveland, Ohio

National Aeronautics
and Space Administration

**Scientific and Technical
Information Office**

1977

COLD-AIR PERFORMANCE OF A 12.766-CENTIMETER-TIP-DIAMETER AXIAL-FLOW COOLED TURBINE

II - EFFECT OF AIR EJECTION ON TURBINE PERFORMANCE

by Jeffrey E. Haas and Milton G. Kofskey

Lewis Research Center and
U.S. Army Air Mobility R&D Laboratory

SUMMARY

As part of a technology program to determine the aerodynamic penalties incurred when coolant air is ejected from the blade surfaces of small turbines, an air cooled version of a 12.766-centimeter-tip-diameter, single-stage, axial-flow turbine was designed, built, and tested to determine the performance over a range of speed, pressure ratio, and air ejection rate.

The turbine design point was based on driving a 10-to-1 pressure ratio compressor at a rotative speed of 70 000 rpm. The turbine inlet temperature was 1478 K. The compressor drive turbine was designed for near optimum work factor and solidity. The stator and rotor blading was designed to provide sufficient room for internal cooling passages. Holes through the stator blade suction surface and slots in the trailing edge of both the stator and rotor blades were provided to allow for the discharge of air from these locations to simulate coolant flow ejection. A primary-to-air ejection temperature ratio of about 1 was maintained.

The results of this investigation indicated a total efficiency of 82.5 percent at equivalent design speed and design specific work. This efficiency was obtained with the air ejection holes and slots plugged. The air ejection holes were then unplugged. At equivalent design values of speed and total pressure ratio and with air ejection rates of 3.3 percent of turbine mass flow for the stator and 3.6 percent for the rotor, the primary and thermodynamic efficiencies were 83.7 percent and 78.5 percent, respectively.

Tests were also conducted where the stator and rotor ejection flow rates were independently varied from 0 to about 10 percent of the turbine mass flow. At equivalent design values of speed and total pressure ratio, there was an approximate 0.2 percent decrease in thermodynamic efficiency with each percent increase in stator ejection flow rate. When the rotor ejection flow was varied, a decrease in thermodynamic efficiency of approximately 0.6 percent per percent ejection flow rate occurred.

INTRODUCTION

Engine performance in terms of specific fuel consumption and specific power or thrust for the small gas turbine engine in the 1-kilogram-per-second mass flow rate and 225- to 375-kilowatt class has not kept pace with that achieved in larger engines. This results from the fact that, as engine size is reduced, it becomes increasingly difficult to maintain geometric similarity with larger engines. That is, such parameters as tip clearance ratio (based on percent of blade height), aspect ratio, and trailing edge blockage must change from established values for larger engines.

To achieve high specific work in a gas turbine engine requires a high compressor pressure ratio and high turbine inlet temperature. A high compressor pressure ratio, together with the small mass flow, results in a turbine design with a small annulus area and thus a small blade height. High turbine inlet temperature (above 1300 K) necessitates the use of internal air cooling, which in turn imposes minimum requirements on stator and rotor blade chord lengths and thicknesses to provide adequate space for internal cooling passages and to maintain structural integrity. The longer chord lengths and smaller blade heights result in a low aspect ratio design.

Reference 1 indicates that a low aspect ratio design results in an efficiency penalty due to increased secondary flow losses. Because of the small blade height, the secondary flow fields encompass a significantly greater portion of the airflow channel than for a larger aspect ratio design and can extend out to the airfoil midspan region, resulting in higher overall losses. Tip clearance losses are more severe because a tip clearance of 1.0 to 1.5 percent of the blade height as commonly achieved in larger engines cannot always be achieved in small turbines from mechanical considerations. Also, minimum manufacturing tolerances become a larger percentage of the blade profile dimensions as the size of the blading is reduced. Together, these effects reduce the level of efficiency in small turbines by as much as five points compared with a large turbine of comparable loading, Mach number, and turning angle.

As part of the small turbine technology program at the Lewis Research Center, a two-phase program was initiated in the 1-kilogram-per-second mass flow rate and 225- to 375-kilowatt class to determine (1) the baseline level of efficiency achievable and (2) the aerodynamic penalties incurred when air is ejected from the blade surfaces to simulate the discharge of cooling air. This program includes both axial- and radial-flow turbines. These turbines were designed for an inlet temperature of 1478 K to drive a two-stage, 10-to-1 pressure ratio compressor with a mass flow of 0.952-kilogram-per-second at a rotative speed of 70 000 rpm. Reference 2 contains detailed aerodynamic design information for this compressor. The single-stage axial turbine designed for this application has a 12.766-centimeter-tip diameter, and near optimum work factor and solidity.

For the purpose of determining the level of achievable aerodynamic performance, a solid blade configuration was selected with the minimum tip clearance and the minimum allowable leading and trailing edge thicknesses from a manufacturing standpoint of solid blades. The resulting design had blade numbers of 56 and 59 for the stator and rotor, respectively. The aspect ratio for both the stator and rotor was one. Reference 3 presents the design and experimental investigation of the solid blade turbine. A total efficiency of 83.2 percent was obtained for the solid blade configuration at both equivalent design values of speed and total pressure ratio and at equivalent values of speed and work factor. This was about 2 percentage points less than design.

To study the aerodynamic penalties incurred with air ejection from the blade surfaces of turbines in this size class, the stator and rotor blading from the solid blade configuration was redesigned. The chord lengths and blade thicknesses were doubled over that of the solid blade configuration to allow sufficient space for internal cooling passages. Holes through the stator blade suction surface and slots in the trailing edge of both the stator and rotor blades were provided to allow for the discharge of air to simulate cooling flow ejection.

This report presents the design and experimental investigation of the aerodynamic performance of the air cooled configuration. The experimental investigation was conducted in two parts. In the first phase of the testing, all of the air ejection holes were plugged and the aerodynamic performance was obtained over a range of speed from 0 to 110 percent of equivalent design speed and over a range of total to static pressure ratio from 1.42 to 5.04. In the second phase of the testing the air ejection holes were unplugged and the aerodynamic performance was obtained for various stator and rotor air ejection rates at equivalent design speed only over a range of total to static pressure ratio from 1.6 to 4.0. In these tests a primary-to-air ejection temperature ratio of about 1 was maintained. In addition, a reference report was used to predict the turbine performance at the design value of primary-to-coolant total temperature ratio of 2.4. The investigations were conducted at turbine inlet total conditions of approximately 8.27 newtons per square centimeter and 310 K.

Performance results are presented in terms of equivalent mass flow, equivalent work, equivalent torque, efficiency, and rotor exit flow angle. Also included are the variation of efficiency with stator and rotor air ejection rates.

SYMBOLS

A area, cm^2

$\Delta h'$ total specific work, J/g

N	rotative speed, rpm
p	absolute pressure, N/cm^2
R	gas constant, J/(kg)(K)
R_x	blade reaction, $\left(W_3^2 - W_2^2\right)/2\,\Delta h'$
r	radius
T	absolute temperature, K
U	blade velocity, m/sec
V	absolute gas velocity, m/sec
ΔV_u	change in absolute tangential velocity, m/sec
W	relative gas velocity, m/sec
w	mass flow, kg/sec
y	coolant fraction, ratio of air ejection flow to primary flow
α	absolute gas flow angle measured from axial direction, deg
β	relative gas flow angle measured from axial direction, deg
γ	ratio of specific heats
δ	ratio of inlet total pressure to U.S. standard sea-level pressure, p'_1/p^*
ϵ	function of γ used in relating parameters to those using air inlet conditions at U.S. standard sea-level conditions, $(0.740/\gamma)[(\gamma + 1)/2]^{\gamma/(\gamma-1)}$
η	efficiency based on total-pressure ratio
η_L	local efficiency (based on local conditions at rotor exit)
η_p	primary efficiency (based on inlet-total- to exit-total-pressure ratio)
η_s	static efficiency (based on inlet-total- to exit-static-pressure ratio)
η_t	total efficiency (based on inlet-total- to exit-total-pressure ratio)
η_{th}	thermodynamic efficiency (based on inlet-total- to exit-total-pressure ratio)
θ_{cr}	squared ratio of critical velocity at turbine inlet temperature to critical velocity at U.S. standard sea-level temperature, $(V_{cr}/V^*_{cr})^2$
τ	torque, N-m
ω	turbine speed, rad/sec

Subscripts:

c	coolant
cr	condition corresponding to Mach number of unity
eq	equivalent
id	ideal
p	primary
plugged	plugged turbine
r	rotor
s	stator
T	total
t	rotor tip
u	tangential component
1	station at turbine inlet (fig. 6)
2	station at stator exit (fig. 6)
3	station at rotor exit (fig. 6)
4	station downstream of rotor exit (fig. 6)

Superscripts:

'	absolute total state
*	U.S. standard sea-level conditions (temperature, 288.15 K; pressure, 10.13 N/cm^2)

COOLED TURBINE DESIGN

The turbine used in this experimental investigation was designed to drive a two-stage, 10-to-1 pressure ratio compressor with a mass flow of 0.952 kilogram per second and a rotative speed of 70 000 rpm. The design turbine inlet temperature was 1478 K. A list of both the engine design conditions and the equivalent design conditions for this turbine are presented in table I. As discussed in the INTRODUCTION, this turbine was designed for near optimum work factor and solidity. To provide sufficient room for internal coolant air passages in the stator and rotor profiles, the chord lengths and blade thicknesses were twice that of the solid blade configuration (ref. 3). Since the same blade heights and solidities were maintained between the two configura-

tions, the aspect ratio and blade number of this coolable blade turbine were half those of the solid blade turbine of reference 3.

The air cooled turbine had a design primary efficiency of 85 percent (assuming no stator or rotor coolant air ejection) which was the same as the design efficiency of the solid blade turbine. This results from the fact that the blading for the air cooled version was scaled from the solid blade configuration.

The turbine was designed with both the stator and rotor blading being untwisted and untapered. The untwisted, untapered design was a compromise to facilitate fabrication of the blade with internal coolant passages. The solid blade turbine was also designed with untwisted and untapered blading.

Selecting an untwisted design can produce an efficiency penalty due to less than optimum rotor incidence, reaction, and radial distribution of specific work compared to a conventional free-vortex (twisted) design. The off-design performance computer program of reference 4 was used to investigate these effects. The results of this program indicated that there would be less than a half point penalty in efficiency by selecting an untwisted design.

The rotor inlet mean camber angle was a constant 40.5°. Thus the design rotor incidence angles were 16.2°, 7.7°, and -6.1° at the hub, mean, and tip, respectively. The design values of rotor reaction R_x were 0.335, 0.440, and 0.512 at the hub, mean, and tip, respectively.

A rotor blade tip clearance of 0.25 millimeter was selected as being the minimum limit for turbines of this size due to mechanical considerations as a result of engine transient conditions. For this turbine, this clearance amounted to 2.4 percent of the blade height. The tip clearance was obtained by use of a recess in the outer casing above the rotor blade tips. In this way, the rotor blade height could be maintained at the full stator passage height. Reference 5 indicated that a recessed casing would reduce the tip clearance losses for a rotor of near impulse design. Even though the subject turbine was not an impulse design, experience indicated that this type of tip clearance configuration would reduce the tip clearance losses.

The number and location of coolant air ejection holes required were selected as being typical of air cooled turbines. A primary-to-coolant flow temperature ratio of 2.4 was selected. For the stator, a single row of film coolant ejection holes located about 15 percent of the suction surface length downstream of the leading edge were used in addition to trailing edge coolant ejection slots. Calculations indicated that 75 percent of the stator coolant air would be ejected from the trailing edge slots and 25 percent ejected from the row of film cooling holes. For the rotor, only trailing edge coolant ejection slots were used. Figure 1 shows the stator and rotor blade profiles and the location of the coolant holes and slots.

Table II compares some physical parameters of the air cooled turbine to the

solid blade turbine. The air cooled configuration had an aspect ratio of 0.50 compared to an aspect ratio of one for the solid blade turbine. The solidities of 1.60 and 1.68 for the stator and rotor, respectively, were nearly the same as the solid blade configuration. There were 28 stator blades and 30 rotor blades compared to 56 stator blades and 59 rotor blades for the solid blade turbine.

Figure 2 shows the velocity diagrams as calculated at the hub, mean and tip diameters. It can be seen that the stator discharge angle was a constant 74.2° and the rotor relative discharge angle was a constant -61.9° from hub to tip.

The blade surface velocities at the hub, mean, and tip diameters, as calculated from the computer program of reference 6, are shown in figure 3 for the stator and rotor. The figure shows that there was no large diffusion predicted for any of the three blade sections.

Figure 4(a) is a photograph of the stator assembly and figure 4(b) is a photograph of the rotor assembly. These photographs show some of the design features of the air cooled turbine blading.

APPARATUS, INSTRUMENTATION, AND TEST PROCEDURE

The apparatus used in this investigation consisted of the subject turbine, an air-brake dynamometer used to absorb and measure the power output of the turbine, an inlet and exhaust piping system including flow controls, and appropriate instrumentation. A schematic of the experimental equipment is shown in figure 5. A cross-sectional view of the turbine giving the instrument measuring station locations is shown in figure 6.

Instrumentation at the turbine inlet (station 1) measured static pressure and total temperature. Static pressures were obtained from eight taps with four on the inner wall and four on the outer wall. The inner and outer taps were located opposite each other at 90° intervals around the circumference at a distance approximately two axial chord lengths upstream of the stator. The temperature was measured with three thermocouple rakes, each containing three thermocouples at the area center radii of three equal annular areas.

At station 3, approximately three axial chord lengths downstream of the rotor, the static pressure, total pressure, total temperature, and flow angle were measured. The static pressure was measured with eight taps with four each on the inner and outer walls. These inner and outer wall taps were located opposite each other at 90° intervals around the circumference. A survey probe was used for measurement of total pressure, total temperature, and flow angle. Figure 7 shows the probe and actuator equipment and also shows a closeup of the probe sensing elements.

There were four total temperature rakes, each containing three thermocouples at the area center radii of three equal annular areas, at station 4 located about 15.7 centimeters downstream from the rotor exit. Temperatures from these rakes were used to calculate turbine efficiency. This efficiency was used to check the turbine efficiency as calculated from torque, speed, and mass flow measurements. The efficiency based on torque is presented in this report.

The rotational speed of the turbine was measured with an electronic counter in conjunction with a magnetic pickup and a shaft-mounted gear. The primary mass flow was measured with a calibrated critical flow nozzle. An airbrake dynamometer absorbed the power output of the turbine. The torque load was measured with a commercial strain-gage load cell.

The stator and rotor air ejection flows were supplied from the laboratory pressurized air system. Both flows were controlled and measured separately. The stator ejection air entered a circumferential plenum over the stator blades, passed into the blades through holes in the blade tips, and then was ejected through the row of holes and trailing edge slots. The rotor ejection air was fed through the casing downstream of the rotor into a hollow rotor disk, through holes in the rotor blade bases and was discharged through the trailing edge slots. Measurement of the stator and rotor air ejection flows was made with calibrated mass flowmeters, which operated on a principle similar to that used in hot-wire anomometry. Measurements of the air ejection static pressure and total temperature were made just upstream of where the air ejection lines were fed into the turbine housing.

In order to obtain aerodynamic performance, friction torque was added to dynamometer torque. The friction torque from the bearings, seal, and coupling windage was obtained by driving the rotor and shaft over the range of speeds covered in this investigation. In order to eliminate disk windage and blade pumping and churning losses from the friction torque, the turbine cavity was evacuated to a pressure of approximately 0.013 newton per square centimeter. A friction torque value of 0.185 newton-meter was obtained at equivalent design rotative speed. This value of friction torque corresponded to 4.0 percent of the torque obtained at equivalent design rotative speed and pressure ratio.

Data were obtained at nominal inlet total flow conditions of 310 K and 8.27 newtons per square centimeter. Turbine inlet total pressure p'_1 was calculated from static pressure, primary-air mass flow, the known annulus area, and the total temperature by the following equation:

$$p_1' = p_1 \left[\frac{1}{2} + \frac{1}{2} \sqrt{1 + \frac{2R(\gamma - 1)}{\gamma} \left(\frac{w_p \sqrt{T_1'}}{p_1 A_1} \right)^2} \right]^{\gamma/(\gamma-1)}$$

Rotor exit total pressure p_3' was similarly calculated by using static pressure, turbine exit flow angle, annulus area, and total temperature, and the total mass flow (primary plus ejection air), as follows:

$$p_3' = p_3 \left\{ \frac{1}{2} + \frac{1}{2} \sqrt{1 + \frac{2R(\gamma - 1)}{\gamma} \left[\frac{(w_p + w_c) \sqrt{T_3'}}{p_3 A_3 \cos \alpha_3} \right]^2} \right\}^{\gamma/(\gamma-1)}$$

The rotor exit total temperature T_3' was derived from the inlet temperature and the enthalpy drop based on torque, mass flow, and speed. The outlet flow angle α_3 was the absolute flow angle measured from the axial direction at the mean radius.

When ejection air is used, two efficiencies are defined: primary efficiency η_p and thermodynamic efficiency η_{th}. In equation form,

$$\eta_p = \frac{\frac{2\pi\tau N}{60}}{w_p \Delta h_{id,\,p}}$$

$$\eta_{th} = \frac{\frac{2\pi\tau N}{60}}{w_p \Delta h_{id,\,p} + w_{c,\,s} \Delta h_{id,\,c,\,s} + w_{c,\,r} \Delta h_{id,\,c,\,r}}$$

Primary efficiency relates the total power output of the primary and ejection air to the ideal power of only the primary flow. The thermodynamic efficiency takes into account the ideal energy of the ejection air. The ideal energy of the stator ejection air is based on the ratio of the inlet total pressure of the stator ejection air (as calculated from measurements of mass flow, flow area, total temperature, and static pressure) to the rotor exit total pressure. Likewise, the ideal energy of the rotor ejection air is based on the ratio of the inlet total pressure of the rotor ejection air to the rotor exit total pressure.

RESULTS AND DISCUSSION

Performance results are presented for a 12.766-centimeter-tip-diameter, single-stage, axial-flow turbine with rotor and stator blade air ejection to simulate coolant flow ejection. Performance tests were made with air as the working fluid at inlet total conditions of approximately 8.27 newtons per square centimeter and 310 K.

The discussion of the performance results will be divided into two sections. The first section will discuss the turbine performance obtained with the surface ejection holes and slots plugged flush with the surface. The results for this part of the investigation shall be referred to as the "plugged" turbine results. The second section will discuss the performance when the ejection holes were unplugged and air ejected from the stator and rotor to simulate coolant ejection at various flow rates. Results for this part of the investigation shall be referred to as the "cooled" turbine results.

Performance with Ejection Holes Plugged

Mass flow. - Figure 8 shows the variation of equivalent mass flow with total- to static-pressure ratio. An equivalent mass flow of 0.275 kilogram per second was obtained at equivalent design values of speed and total- to static-pressure ratio (3.16). This mass flow was 11.8 percent larger than the design value of 0.246 kilogram per second. Measurements indicated that the stator throat area was about 11.5 percent larger than that required to pass design primary mass flow. This anomaly was due to a fabrication error in the blade setting angle. Fabrication errors of this nature are common in small turbomachinery designs. This 11.5 percent larger stator throat area corresponded to a difference in the mean throat dimension of about 0.051 centimeter or about 2.5° in blade setting angle.

The rotor throat area was also found to be about 9.0 percent larger than design. The stator- to rotor-throat area ratio was calculated to be 2.6 percent higher than the design value. This area and area ratio mismatch resulted in the turbine operating with different velocity diagrams than design. This difference in velocity diagrams will be discussed in further detail in the section Turbine efficiency.

Figure 9 shows the variation of turbine total pressure ratio with turbine inlet-total- to exit-static-pressure ratio for lines of constant speed. This figure was included in the report as a reference curve for the reader.

Equivalent torque. - Figure 10 shows the variation of equivalent torque with total- to static-pressure ratio for lines of constant speed. An equivalent torque value of 4.96 newton-meter was obtained at equivalent design values of speed and total- to static-pressure ratio. This was about 6.9 percent larger than design. The percentage

increase in torque was not as large as the percentage increase in mass flow. This means that the change in tangential momentum across the rotor was less than design. Therefore, the turbine total efficiency was less than the design value. The torque curves show that limiting loading was not reached even though pressure ratios considerably higher than design were obtained.

Rotor exit flow angle. - Figure 11 shows the variation of rotor exit flow angle as a function of pressure ratio for lines of constant equivalent speed. The flow angles were measured at the mean radius and from the axial direction. Negative angles indicate a positive contribution to specific work. At equivalent design values of speed and total- to static-pressure ratio, the mean-radius exit flow angle was about 0°. The velocity diagrams of figure 2 show that the turbine was designed for a mean-radius exit flow angle of -17.5°. This difference will be discussed in the next section.

Radial survey results. - Figure 12 shows experimental data and calculated results from a rotor exit radial survey conducted at equivalent design speed and near design total pressure ratio. This survey was conducted at one circumferential position approximately 1.8 centimeters downstream of the rotor. Levels of total pressure (fig. 12(a)) were adjusted to provide agreement with the measured turbine mass flow. Levels of total temperature (fig. 12(b)) were adjusted to correspond to the average work calculated from torque, speed, and mass flow. A linear variation in static pressure between the hub and tip values was assumed. Figure 12 shows large radial variations in the experimental data and calculated results.

The interpretation placed on these survey results must be qualified based on the experimental results of reference 7. In this reference investigation, radial and circumferential surveys were made downstream of a single-stage turbine rotor. The experimental results indicated large radial and circumferential gradients in the total temperature and total pressure measurements. The circumferential gradients were attributed to circumferential gradients introduced by the stator. The radial gradients are caused by both the stator and rotor. Since the rotor exit radial survey for the subject turbine was conducted at only one circumferential location, the stator-induced circumferential variations in the flow conditions were not accounted for. Therefore, discussion of figure 12 will consider only the trends in the flow conditions as they existed at that one circumferential location.

These trends can be summarized as follows: A region of low total pressure (fig. 12(a)), total temperature (fig. 12(b)) and efficiency (fig. 12(c)) existed at the hub and extended to near the midspan. This region was believed to be caused by large loss accumulations at the stator hub which persisted through the rotor. The radial variation in rotor exit absolute flow angle (fig. 12(d)) showed a large region of low turning near the rotor midspan as compared to the hub and tip in the region of high efficiency. The variation in rotor exit relative flow angle (fig. 12(e)) also showed a region of flow

underturning near the rotor midspan, in conjunction with flow overturning near the endwalls. The measured rotor blade exit mean camber angle for the subject rotor is also shown in figure 12(e). The observed variations in absolute and relative flow angles can be explained with the following rotor secondary flow model. In this rotor secondary flow model, the relatively high efficient free stream flow sets up blade-to-blade static pressure gradients which overwhelm the blade-to-blade static pressure gradients set up by the lower momentum flow near the end walls. This results in vortices which cause flow overturning near the end walls and flow underturning in the midspan region. The presence of these rotor vortices was reported in reference 8.

Figure 13 shows the velocity diagrams at the hub, mean, and tip as calculated from the experimental results at equivalent design speed and near design total pressure ratio. As with figure 12, the discussion of the experimental velocity diagrams must be qualified because the diagrams are valid only for the circumferential location where the radial rotor exit survey was made. For the velocity diagram calculations, a stator total pressure loss of 5 percent was assumed. These experimental diagrams were compared to the design velocity diagrams of figure 2. The experimental rotor incidence angles were 14.0°, 2.8°, and -14.6° at the hub, mean, and tip, respectively, compared to design values of 16.2°, 7.7°, and -6.1°. The experimental values of rotor reaction R_x were 0.372, 0.234, 0.588 at the hub, mean, and tip, respectively, compared to design values of 0.335, 0.440, and 0.512. The large deviation in the reaction at the mean section from the design value might be due to overexpansion of the stator core flow, which in turn would cause a reduced level of reaction across the rotor.

Turbine efficiency. - An experimental turbine performance map for the plugged turbine is shown in figure 14. This map shows equivalent specific work output $\Delta h'/\theta_{cr}$ as a function of the mass flow-speed parameter $\epsilon w\omega/\delta$ for the various equivalent speeds investigated. Lines of constant pressure ratio and efficiency are superimposed. Figure 14(a) shows the performance of the turbine based on total conditions across the turbine. A total efficiency of 82.5 percent was obtained at equivalent design values of speed and specific work. A total efficiency of 82.8 percent was obtained at equivalent design values of speed and total pressure ratio.

Over the range of pressure ratio and speeds investigated, the total efficiency varied from 55 percent near the 30 percent speed line to 84 percent at the 110 percent speed line. Figure 14(b) shows the performance map based on inlet-total- to exit-static-pressure ratio. At the condition corresponding to equivalent design values of speed and specific work, the static efficiency was about 72.5 percent. Since the total efficiency was 82.5 percent for this same operating point, there was 10.0 percentage points in efficiency due to rotor exit kinetic energy.

A comparison between the efficiencies of the solid blade configuration (ref. 3) and

the plugged turbine configuration should give an indication of the effect of reduced aspect ratio. In order to obtain a valid basis for comparison, the anomalies in the stator- to rotor-throat-area ratios for both configurations were accounted for. Experimentally, there was a 0.7 percentage point difference between the two configurations. In reference 3, it was reported that the solid blade configuration had a stator- to rotor-throat-area ratio that was 5.5 percent smaller than design. As indicated in reference 3, opening the stator throat area would shift the efficiency contours on the performance map in the direction of decreased speed. This shift would amount to an increase of about 1 percentage point at equivalent design values of speed and pressure ratio and, therefore, an efficiency of about 84 percent was projected for the solid blade configuration.

For the plugged turbine the stator throat area would have to be closed to obtain the design stator- to rotor-throat-area ratio. The computer program of reference 4 projected a decrease in efficiency of about half a percentage point by closing the stator throat area. This is equivalent to the efficiency contours on the performance map shifting in the direction of increased speed. This shift would amount to a decrease of about half a percentage point at equivalent design values of speed and pressure ratio and, therefore, an efficiency of about 82 percent was projected for the plugged turbine configuration. This was 2 percentage points less than the projected efficiency for the solid blade turbine of reference 3.

The performance estimation method of reference 9 was used to determine what the predicted difference would be between the two configurations. This method calculates an overall efficiency based on the values of profile loss, secondary loss, tip clearance loss, and trailing edge loss in the stator and rotor. This method predicted an efficiency difference of about 2 percentage points. The major cause of this difference was attributed to an increased secondary flow loss for the plugged turbine because of the decreased aspect ratio.

Performance with Air Ejection

The turbine aerodynamic performance with air ejection was obtained with three modes of stator air ejection. Initially, the air was ejected from both the stator film cooling holes and trailing edge slots (Mode I). Next, the trailing edge slots were plugged and air was ejected from only the row of film cooling holes (Mode II). Finally, the film cooling holes were plugged and air was ejected from only the trailing edge slots (Mode III). In all three modes, air was also ejected from the trailing edge slots in the rotor. For the following discussion the three modes of stator air ejection will be referred to by their mode numbers.

For each mode, data were first obtained over a range of total- to static-pressure

ratio from about 1.6 to 4.0 at equivalent design speed with the stator and rotor ejection air total pressure equal to the turbine inlet total pressure. Then, at equivalent design speed and design total pressure ratio, the stator or rotor ejection rate was held constant and the ejection rate through the other blade row was varied over a range from zero to about 10 percent of the primary air flow. In all of the above tests, the data were obtained at a primary-to-ejection air temperature ratio of about 1.1.

Mass flow. - Figure 15 shows the variation of equivalent primary mass flow with total- to static-pressure ratio at equivalent design speed for Mode I. Supplying the stator and rotor ejection air at a pressure equal to the turbine inlet total pressure resulted in a stator ejection air fraction y_s of 0.033 and a rotor ejection air fraction y_r of 0.036. The figure shows that with a constant 3.3 percent stator ejection air flow, the primary air flow was smaller than that obtained for the plugged turbine case. At design pressure ratio (3.16), the difference in primary mass flow between the plugged turbine and Mode I was 4.1 percent. This difference between the primary flow reduction (4.1 percent) and the amount stator air ejection (3.3 percent) will be discussed in detail in a following section.

Turbine efficiency. - Figure 16 shows the variation of primary and thermodynamic efficiency with total pressure ratio at equivalent design speed for Mode I. The stator and rotor ejection air fractions were maintained constant at 0.033 and 0.036, respectively. At design total pressure ratio, the primary efficiency was 83.7 percent and the thermodynamic efficiency was 78.5 percent. Thus, the primary efficiency was 0.9 percentage points greater, and the thermodynamic efficiency 4.3 percentage points less than the total efficiency of 82.8 obtained for the plugged turbine.

Figure 17 shows the variation in efficiency with air ejection rate at equivalent design speed and design total pressure ratio for Mode I. Figure 17(a) shows the variation in efficiency with stator air ejection rate when the rotor air ejection rate was maintained at a constant 3.6 percent. Figure 17(b) shows the variation in efficiency with rotor air ejection rate when the stator air ejection rate was maintained at a constant 3.3 percent. Figure 17(a) shows an approximate 0.9 percent increase in primary efficiency and an approximately 0.2 percent decrease in thermodynamic efficiency with each percent increase in stator air ejection rate.

Figure 17(b) shows an approximate 0.5 percent increase in primary efficiency with each percent increase in rotor air ejection rate. As mentioned in reference 10, this variation in primary efficiency is an indication of the net torque increase contributed to the rotor by air ejection. The net torque is affected by two factors. A positive contribution to torque results from jet-reaction work being done by the rotor ejection air as the flow exits from the trailing edge. However, some torque is absorbed in pumping the rotor ejection air up to blade speed. If the jet reaction power is greater than the pumping power, a net increase in torque, and primary efficiency will result. For this

turbine, a net increase in torque existed over the entire range of rotor air ejection rates investigated.

The variation in thermodynamic efficiency in figure 17(b) was an approximate 0.6 percent decrease in efficiency with each percent increase in rotor air ejection rate. This rate of decrease was triple that of figure 17(a), indicating that the rotor ejection air was far less efficient than the stator ejection air.

Performance Comparison of the Three Stator Air Ejection Modes

Figure 18(a), (b), and (c) presents the variations of stator ejection air fraction, equivalent primary flow, and equivalent total flow as a function of the ratio of stator ejection air total pressure to the turbine inlet total pressure $p'_{c,\,s}/p'_1$ for the three modes of stator air ejection. These results were obtained at equivalent design speed and design stage total pressure ratio with a constant 3.6 percent rotor ejection air.

Figure 18(a) shows that stator ejection air fraction increased with pressure ratio for all three modes. At a pressure ratio of one, approximately 77 percent of the total ejection air was ejected from the trailing edge slots (Mode III) and 23 percent was ejected from the film cooling holes (Mode II). As mentioned in the section COOLED TURBINE DESIGN, the design split was 75 percent for the trailing edge slots and 25 percent for the film cooling holes. The dashed curve in figure 18(a) indicates the sum of the Mode II and Mode III flows. Ideally, there should be no discrepancy between this dashed curve and Mode I. However, a difference did exist. If the filler material used in the trailing edge slots for the Mode II tests was not completely removed prior to the Mode III tests, such a discrepancy could arise. A film thickness of only 13 micrometers would reduce the trailing edge slot flow area by about 10 percent. Thus, it is highly probable that the trailing edge slot flow for Mode III was lower than for Mode I. However, this should not affect the qualitative conclusions derived from this data.

Figure 18(b) shows a trend of decreasing equivalent primary flow for all three modes as the pressure ratio increased. Furthermore, at a given pressure ratio, the primary flow was lowest for Mode I and highest for Mode III. This reduction in primary flow was caused by blockage associated with the ejected flow. The greater the ejected flow, the greater the blockage.

Figure 18(c) shows the trend of equivalent total flow for all three modes with pressure ratio. Equivalent total flow is defined as the sum of the actual primary flow and the stator ejection airflow corrected from the turbine inlet total conditions to standard sea-level conditions.

Total flow at a given pressure ratio was highest with Mode III and lowest for

Mode II. The range between the highest and lowest flow was only about 1 percent of total flow. Total flow for Mode II appeared to be constant with increasing pressure ratio, while Modes I and III showed a very slight decrease followed by a small increase. Total flow for Modes I and II was lower than that for the plugged turbine. At a pressure ratio between 1.8 and 1.9, the Mode III total flow equalled that of the plugged turbine.

One possible explanation for these trends may be found from the continuity equation. At sonic conditions a minimum area is required to pass a given mass flow. At less than sonic conditions, the area required to pass the given mass flow is larger. Therefore, at low pressure ratios the ρV of the ejected flow must be lower than that of the primary flow, so that the area required to pass the ejected flow was larger than the area required to pass the same amount of mass flow at the primary mass flow valve of ρV. Thus, the percentage reduction in primary flow was greater than the ejection air fraction. As pressure ratio increased, the ρV of the ejected flow increased, thus reducing the difference in ρV between the two flow rates. If ρV of the ejected flow becomes high enough, the percentage reduction in primary mass flow can equal or be less than the ejection air fraction. Over the range of pressure ratio tested, the total flow for Modes I and II did not attain the plugged turbine value. This occurred since the ρV of the air being ejected from the film cooling holes was not high enough to allow for the ejection air fraction to equal or be greater than the percentage decrease in the primary mass flow.

Figure 19 presents the variations in equivalent torque and mean-radius, average change in tangential momentum across the rotor as a function of pressure ratio. As with the previous figure, these results were obtained at equivalent design speed and design stage pressure ratio with a constant 3.6 percent rotor ejection air. Figure 19(a) shows that the torque for Modes I and III increased with pressure ratio. The torque for Mode I was lower than for Mode III. The two curves were similar with an almost constant difference between them. This constant difference appeared to be the result of a constant loss in torque associated with Mode II.

The change in mean-radius, average tangential momentum ΔV_u, shown in figure 19(b), was calculated from the total flow and torque. The difference in ΔV_u between the plugged turbine and Modes I and III decreased as pressure ratio increased. The ΔV_u for Mode III equalled that of the plugged turbine at a pressure ratio of about 1.9. On the other hand, the difference in ΔV_u between the plugged turbine and Mode II remained relatively constant with pressure ratio. It was noted that summing the differences in ΔV_u between the plugged turbine and Modes II and III approximately equalled the difference in ΔV_u between the plugged turbine and Mode I. A hypothesis for the internal flow that results in these trends is as follows. At a pressure ratio of one, the level of ΔV_u for all three modes was lower than that of the plugged turbine. The

lower ΔV_u for Mode III was unexpected, since reference 11 found that trailing edge ejection fills in the stator wakes, thereby reducing the losses. Therefore, the decrease in ΔV_u for Mode III must result from a decrease in the total flow compared to the plugged turbine. The lower total flow results in the rotor reaction being different between the plugged turbine and Mode III. This in turn causes a difference in the velocity diagrams, and therefore a lower ΔV_u. As the pressure ratio increased for Mode III, the kinetic energy of the total flow at the stator exit increased, thereby increasing the rotor inlet relative total pressure. This caused an increase in the rotor inlet and rotor exit tangential velocity, and thus, the ΔV_u increased. On the other hand, since there was a constant difference in ΔV_u between the plugged turbine and Mode II, there appeared to be no benefit derived from an increase in kinetic energy of the flow ejected from the film cooling holes.

When the trends associated with Modes II and III were combined, they tended to equal the results obtained for Mode I. This indicates there was no interacting effect between Modes II and III. It was also concluded that there was only a small effect on the torque level caused by the 3.6 percent rotor ejection air. If the rotor ejection air had significantly affected the torque (and thus ΔV_u), the sum of the differences in ΔV_u between the plugged turbine and Modes II and III would not have been close to the difference in ΔV_u between the plugged turbine and Mode I.

Comparison of Thermodynamic Efficiency Levels Between Large and Small Aspect Ratio Turbines

A comparison was made of the percentage decreases in thermodynamic efficiency between the subject turbine and the turbine of reference 10 to provide an indication of the relation between air ejection losses and turbine aspect ratio. The reference 10 turbine had a blade height of about 10.2 centimeters and a rotor aspect ratio of 1.75. In this reference investigation, the stator and rotor air ejection fractions were 0.0512 and 0.0638, respectively. The thermodynamic efficiency was 0.874 and the efficiency for the solid (uncooled) blading was 0.923. As was mentioned previously, the thermodynamic and plugged turbine efficiencies for the subject turbine were 0.785 and 0.828, respectively. Thus, the efficiencies for the reference 10 turbine were about 9.0 percentage points higher than the respective efficiencies for the subject turbine.

Figure 20 shows the percentage decrease in thermodynamic efficiency from the uncooled turbine efficiency for the subject and reference 10 turbines. These percentage decreases are based on a 1 percent total air ejection fraction. Since the reference 10 turbine had only trailing edge ejection from both the stator and rotor, the

Mode III case for the subject turbine would provide the best comparison. Figure 20 shows that the percentage decrease in thermodynamic efficiency was 0.64 for Mode III and 0.46 for the reference 10 turbine. Thus, not only was the level of thermodynamic efficiency higher for the reference 10 turbine, but also the loss associated with the ejection air was lower. This could indicate that the additional losses associated with low aspect ratio turbines also compound the loss effects due to the stator and rotor ejection air.

Performance Prediction at Actual Primary-to-Coolant Total Temperature Ratio

The performance results presented in this report were obtained at a primary-to-coolant total temperature ratio near one. The analytical method of reference 12 was used to predict the stator and rotor coolant mass flow fractions and the primary and thermodynamic efficiencies that would exist at a primary-to-coolant total temperature ratio of 2.4. This represents the actual engine temperature ratio. This method assumes that the performance is modeled if the coolant-to-primary momentum ratio is maintained constant between the engine operating case and the reduced temperature ratio case. Specifically, for the subject turbine, the rotor blade coolant to rotor inlet absolute momentum ratio was assumed constant. The absolute momentum ratio is maintained constant if the coolant to rotor inlet absolute total pressure ratio is constant.

Figure 21 shows the results that would be obtained at a temperature ratio of 2.4. In this case, the stator and rotor coolant fractions would be 5.2 percent and 7.2 percent, respectively. In addition, the primary and thermodynamic efficiencies would be 82.2 percent and 78.5 percent, respectively. Thus, the primary efficiency would decrease and the thermodynamic efficiency would remain the same compared to the reduced temperature ratio results.

Comparison of Solid and Cooled Blade Turbine Performance

Table III lists some of the performance parameters for the four different turbine configurations tested in this small turbine program. As was stated in the INTRODUCTION, the purpose of this test program was to study the aerodynamic penalty incurred when air is ejected from the stator and rotor blade surfaces. Table III shows that there was an approximate 5 percentage point decrease in thermodynamic efficiency from the solid blade configuration of reference 3 to the cooled blade configuration with stator and rotor ejection air flows. The actual difference was 6 percentage points when

corrections are made for the stator-rotor throat area ratio anomalies mentioned earlier. Of this difference about 2 percentage points were attributed to the reduced aspect ratio, and about 4 percentage points were attributed to the aerodynamic penalties incurred with the stator and rotor air ejection flow.

CONCLUDING REMARKS

The experimental results obtained from this investigation indicated that the efficiency levels associated with low aspect ratio, cooled turbines are low. Future low aspect ratio turbine designs should perhaps consider the use of contoured stator endwalls and nonfree vortex velocity diagrams to help reduce the effect of secondary flow losses. In addition, if stator cooling air is required, the air should be ejected only from the trailing edge, if possible, to reduce the losses associated with cooling air ejection.

SUMMARY OF RESULTS

An experimental investigation was conducted on a 12.766-centimeter-tip-diameter, single-stage, axial-flow turbine over a range of speed and pressure ratio. The purpose of this investigation was to study the aerodynamic penalties incurred with air injection from the blade surfaces to simulate the effect of cooling air discharge. This turbine was the air cooled version of a compressor drive turbine designed for a 10-to-1 pressure ratio compressor. The design turbine inlet temperature was 1478 K. The turbine was designed for near optimum work factor and solidity. The stator and rotor blading was designed to allow for internal cooling passages. Holes through the stator blade suction surface and trailing edge slots in both the stator and rotor blades allowed for the discharge of air to simulate the effect of cooling air ejection. A primary-to-air ejection temperature ratio of about 1 was maintained.

The experimental investigation of this configuration was conducted in two parts. In the first part all of the air ejection holes were plugged. In the second part the air ejection holes were unplugged and the performance was obtained for various stator and rotor air ejection rates.

The results of this investigation can be summarized in the following sections.

Air Ejection Holes Plugged

1. A total efficiency of 82.5 percent was obtained at equivalent design values of speed and specific work. At equivalent design values of speed and total pressure ratio the total efficiency was 82.8 percent.

2. The total efficiency for this configuration was 2 percentage points less than the total efficiency for the solid blade configuration of reference 3. The difference was attributed primarily to an increased secondary flow loss for the cooled blade configuration due to a smaller aspect ratio.

3. The stator-rotor throat area ratio was 2.8 percent larger than design. A turbine off-design performance computer program predicted that this mismatch would cause an efficiency penalty of about half a percentage point.

Air Ejection Holes Open

1. At equivalent design values of speed and total pressure ratio and with 3.3 percent stator and 3.6 percent rotor air ejection rates, the primary and thermodynamic efficiencies were 83.7 percent and 78.5 percent, respectively.

2. At equivalent design values of speed and total pressure ratio and with a constant 3.6 percent rotor ejection rate, there was an approximate 0.2 percent decrease in thermodynamic efficiency with each percent increase in stator ejection rate. When the stator ejection rate was maintained at a constant 3.3 percent, there was an approximate 0.6 percent decrease in thermodynamic efficiency with each percent increase in rotor ejection rate.

3. The difference in thermodynamic efficiency between the cooled blade configuration with stator and rotor ejection air and the solid blade configuration of reference 3 was approximately 6 percentage points. Of this difference about 2 percentage points were attributed to the reduced aspect ratio, and about 4 percentage points were attributed to the aerodynamic penalties incurred with the stator and rotor air ejection.

Lewis Research Center,
National Aeronautics and Space Administration,
and
U.S. Army Air Mobility R&D Laboratory,
Cleveland, Ohio, May 18, 1977,
505-04.

REFERENCES

1. Ewen, J. S.; Huber, F. W.; and Mitchell, J. P.: Investigation of the Aerodynamic Performance of Small Axial Turbines. ASME Paper 73-GT-3, Apr. 1973.

2. Bryce, C. A.; et al.: Advanced Two-Stage Compressor Program: Design of Inlet Stage. (AT-6133-R, AiResearch Mfg. Co.; NAS3-15324.) NASA CR-120943, 1973.

3. Haas, Jeffrey E.; and Kofskey, Milton G.: Cold-Air Performance of a 12.766-Centimeter-Tip-Diameter Axial-Flow Cooled Turbine. I - Design and Performance of a Solid Blade Configuration. NASA TN D-7881, 1975.

4. Flagg, E. E.: Analytical Procedure and Computer Program for Determining the Off-Design Performance of Axial Flow Turbines. NASA CR-710, 1967.

5. Kofskey, Milton G.: Experimental Investigation of Three Tip-Clearance Configurations over a Range of Tip Clearance Using a Single-Stage Turbine of High Hub-to-Tip Radius Ratio. NASA TM X-472, 1961.

6. Katsanis, Theodore: FORTRAN Program for Calculating Transonic Velocities on a Blade-to-Blade Stream Surface of a Turbomachine. NASA TN D-5427, 1969.

7. Wong, Robert Y.; Miser, James W.; and Stewart, Warner L.: Qualitative Study of Flow Characteristics Through Single-Stage Turbines as Made from Rotor-Exit Surveys. NACA E55K21, 1956.

8. Kofskey, Milton G.; and Allen, Hubert W.: Investigation of a 0.6 Hub-Tip Radius-Ratio Transonic Turbine Designed for Secondary-Flow Study. IV - Rotor Loss Patterns as Determined by Hot-Wire Anemometers with Rotor Operating in a Circumferentially Uniform Inlet Flow Field. NACA RM E58B27, 1958.

9. Ainley, D. G.; and Mathieson, C. G. R.: A Method of Performance Estimation for Axial-Flow Turbines. R. & M. No. 2974, British A. R. C., 1957.

10. Schum, Harold J.; et al.: Cold-Air Experimental Investigation of a Turbine with Blade Trailing-Edge Coolant Ejection. I - Single-Stage Turbine. NASA TM X-3214, 1975.

11. Moffitt, Thomas P.; et al.: Summary of Cold-Air Tests of a Single-Stage Turbine with Various Cooling Techniques. NASA TM X-52968, 1971.

12. Goldman, Louis J.: Cooled-Turbine Aerodynamic Performance Prediction from Reduced Primary to Coolant Total-Temperature-Ratio Results. NASA TN D-8312, 1976.

TABLE I. - TURBINE DESIGN CONDITIONS

Parameter	Engine	Equivalent
Turbine inlet temperature, T'_1, K	1478	288.2
Turbine inlet pressure, p'_1, N/cm^2	91.2	10.1
Mass flow rate, w, kg/sec	0.952	0.246
Rotative speed, N, rpm	70 000	31 460
Specific work, $\Delta h'$, J/g	307.3	62.1
Torque, τ, N-m	39.91	4.64
Power, kW	293	15
Inlet- to exit-total-pressure ratio, p'_1/p'_3	2.57	2.77
Inlet-total- to exit-static-pressure ratio, p'_1/p_3	2.92	3.16
Total efficiency, η_t	0.85	0.85
Work factor, $\Delta V_u/U$	1.67	1.67

TABLE II. - COMPARISON OF TURBINE PHYSICAL PARAMETERS

Parameter	Stator	Rotor	Stator	Rotor
	Cooled configuration		Solid blade configuration (ref. 3)	
Actual chord, cm	2.102	2.102	1.051	1.051
Axial chord, cm	1.607	2.062	0.721	0.968
Leading edge radius, cm	0.152	0.081	0.051	0.028
Trailing edge radius, cm	0.030	0.036	0.010	0.013
Radius				
Hub	5.331	5.331	5.331	5.331
Mean	5.857	5.857	5.857	5.857
Tip	6.383	6.383	6.383	6.383
Blade height, cm	1.051	1.051	1.051	1.051
Solidity	1.60	1.71	1.60	1.68
Aspect ratio	0.50	0.50	1.00	1.00
Number of blades	28	30	56	59
Radius ratio	0.835	0.835	0.835	0.835

TABLE III. - COMPARISON OF SOLID AND COOLED BLADE TURBINE PERFORMANCE

Turbine	Pressure ratio, p'_1/p'_3	Equivalent torque, N-m	Equivalent primary flow, kg/sec	Coolant rate		Efficiency			
				Stator	Rotor	Primary		Thermodynamic	
						Experimental	Corrected	Experimental	Corrected
1 - Design for solid and cooled blade configurations	2.77	4.64	0.246	-----	-----	0.850	0.850	0.850	0.850
2 - Solid blade (ref. 3)		4.27	.231	-----	-----	.832	.840	.832	.840
3 - Cooled blade (coolant holes plugged)		5.06	.275	-----	-----	.828	.823	.828	.823
4 - Cooled blade (coolant holes open)		4.93	.263	0.033	0.036	.837	.832	.785	.780

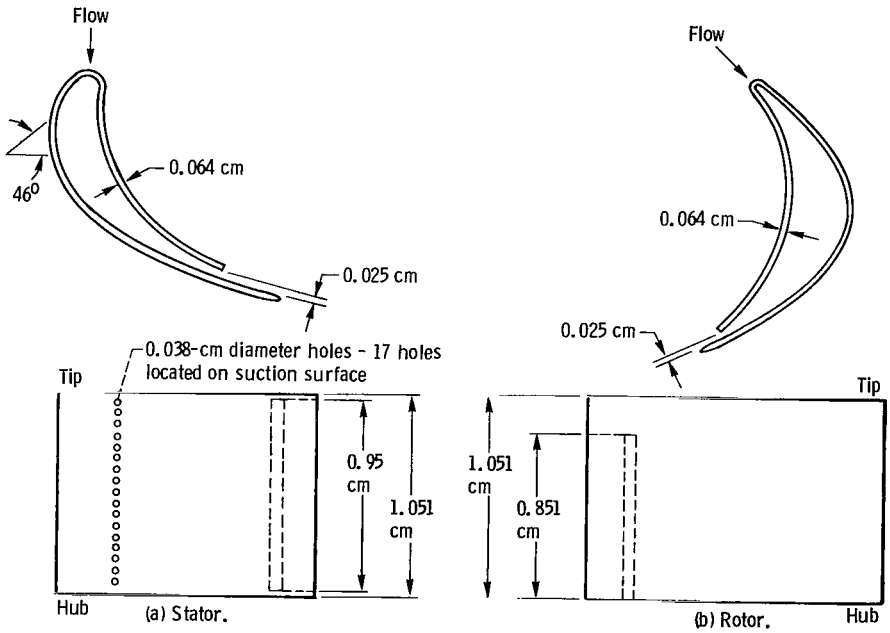

Figure 1. - Arrangement of stator and rotor blade coolant air holes, and slots.

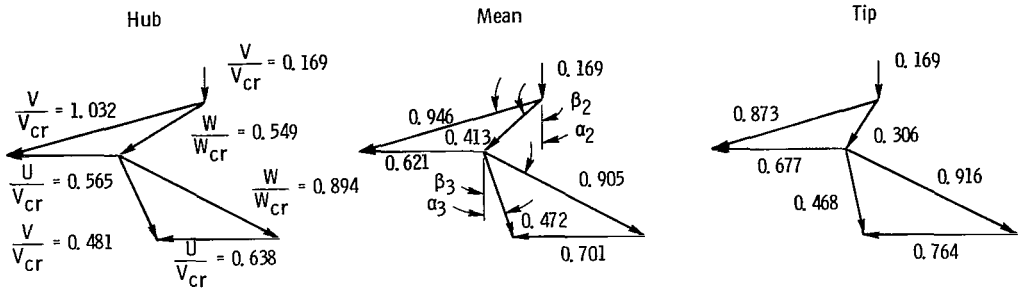

Station	Hub	Mean	Tip
1, Stator entrance			
2, Stator exit			
3, Rotor exit			
Radius (cm) at -			
Station 1	5.33	5.86	6.38
Station 2	5.33	5.86	6.38
Station 3	5.33	5.86	6.38
α_2, deg	74.2	74.2	74.2
β_2, deg	56.7	48.2	34.4
α_3, deg	-23.3	-17.5	-11.6
β_3, deg	-61.9	-61.9	-61.9

Figure 2. - Design velocity diagrams.

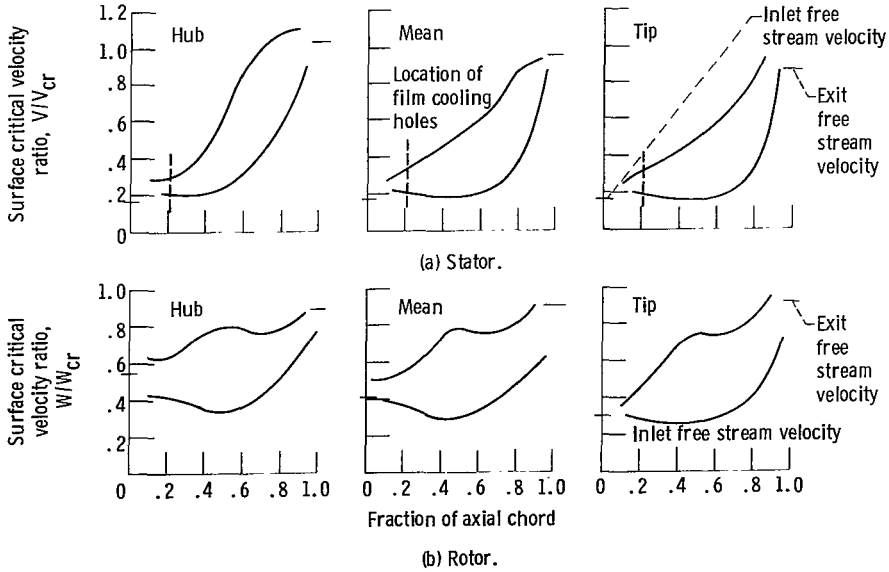

Figure 3. - Design blade surface velocity distributions at hub, mean, and tip.

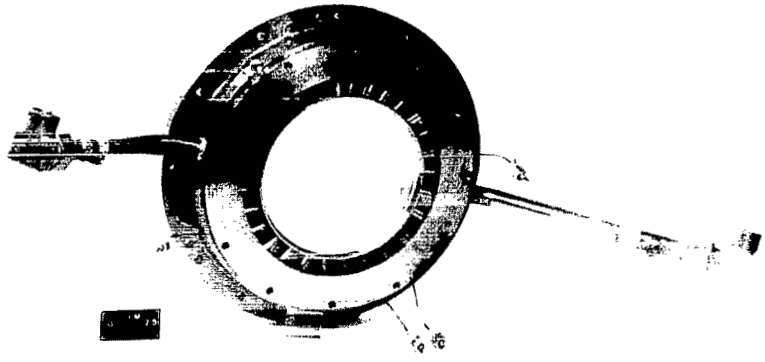

(a) Stator assembly.

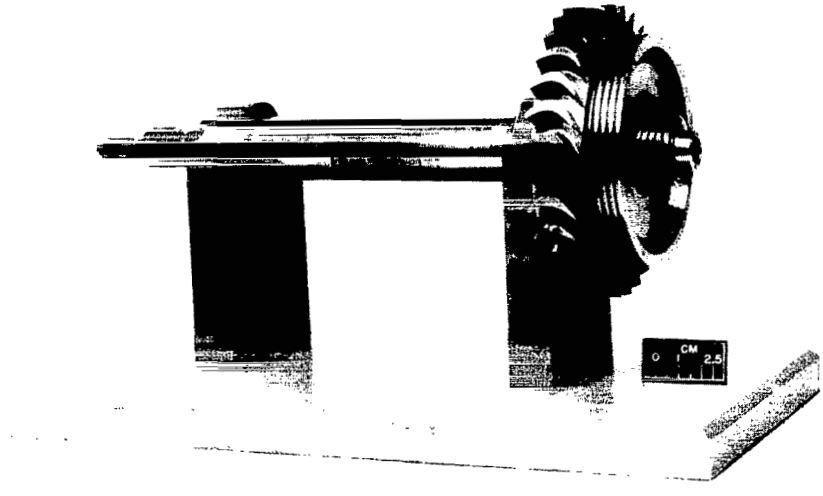

(b) Rotor assembly.

Figure 4. - Turbine test hardware.

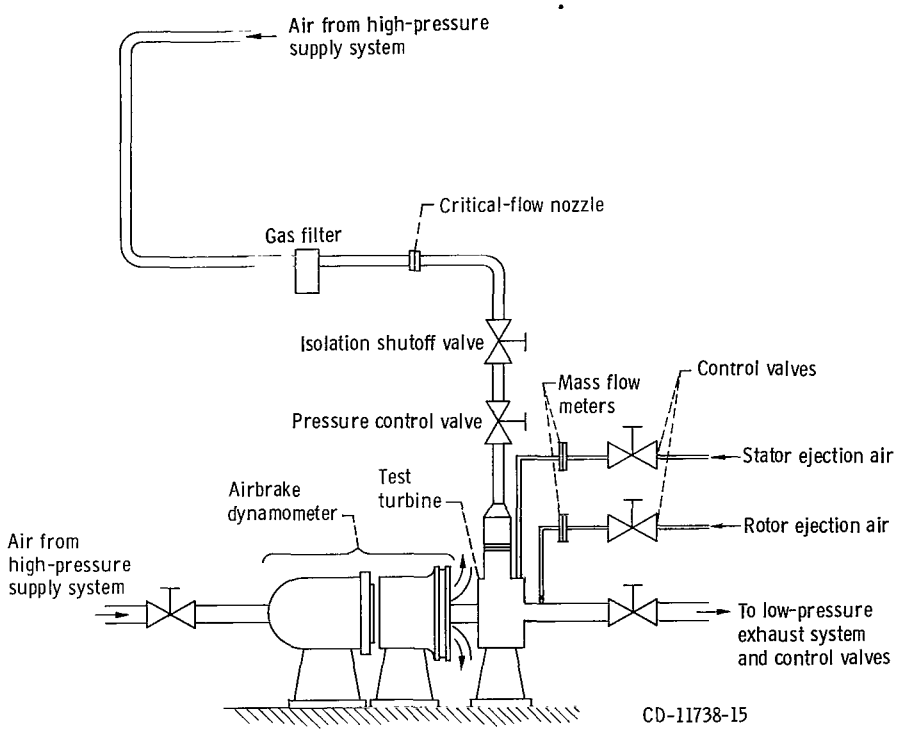

Figure 5. - Experimental equipment.

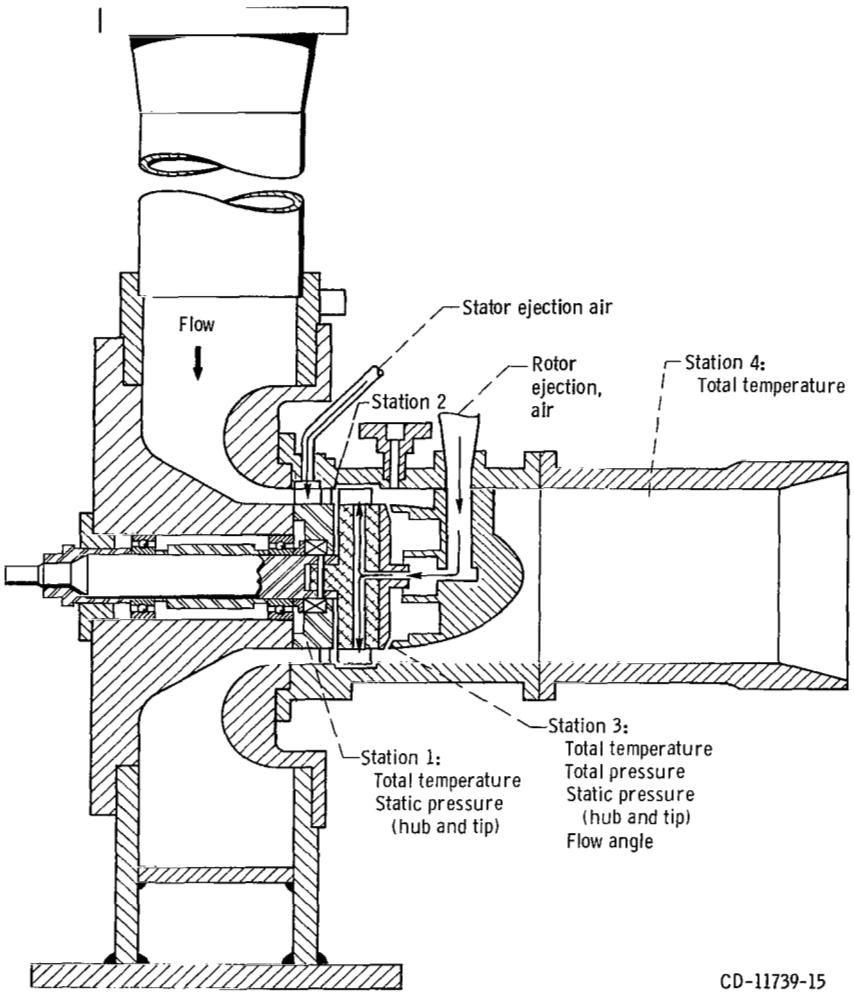

Figure 6. - Schematic of turbine.

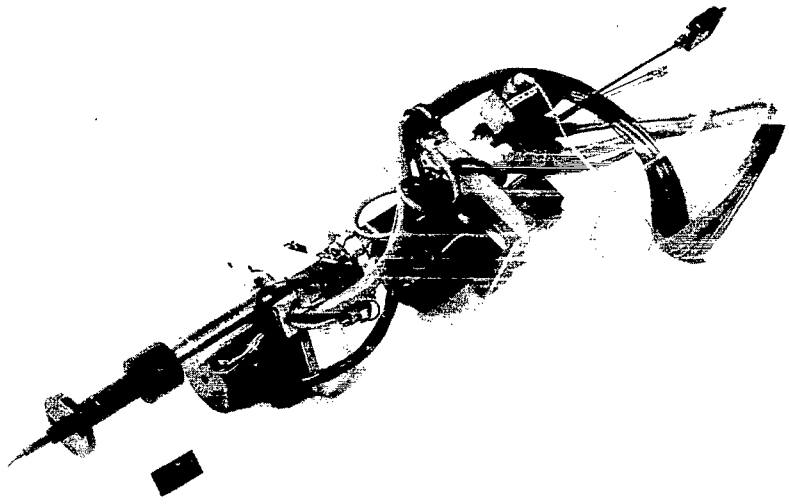

(a) Probe inserted in actuator.

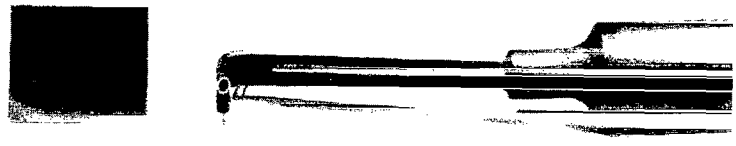

Figure 7. - Probe and actuator equipment used for rotor exit radial surveys.

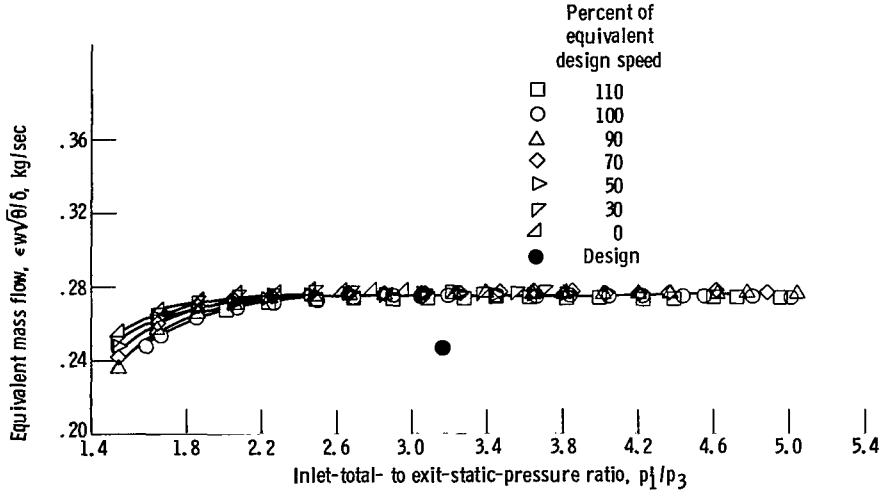

Figure 8. - Variation of mass flow with pressure ratio and speed for plugged turbine.

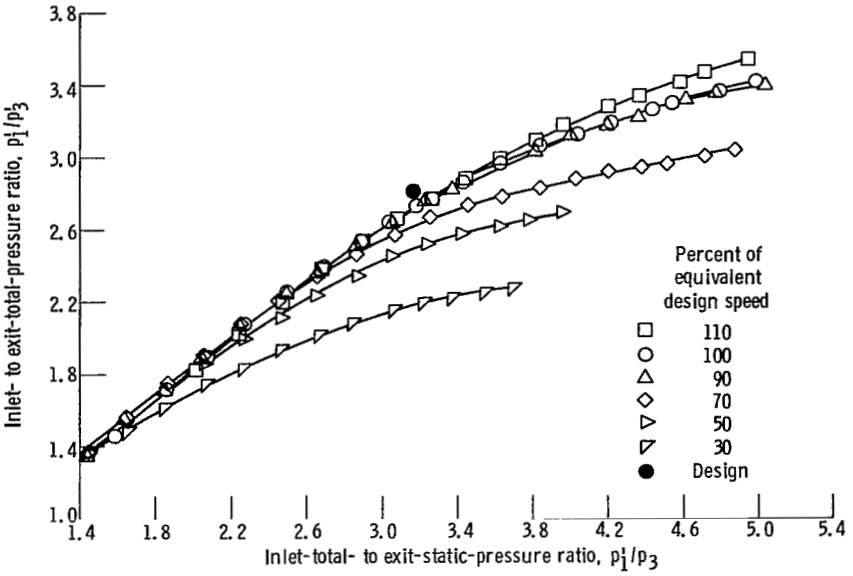

Figure 9. - Variation of total pressure ratio with total to static pressure ratio for plugged turbine.

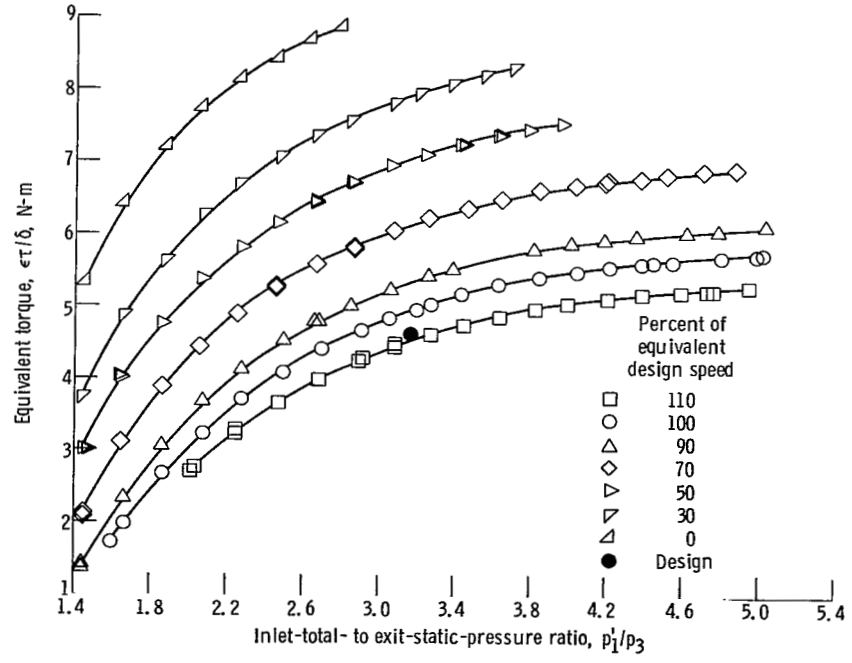

Figure 10. - Variation of torque with pressure ratio and speed for plugged turbine.

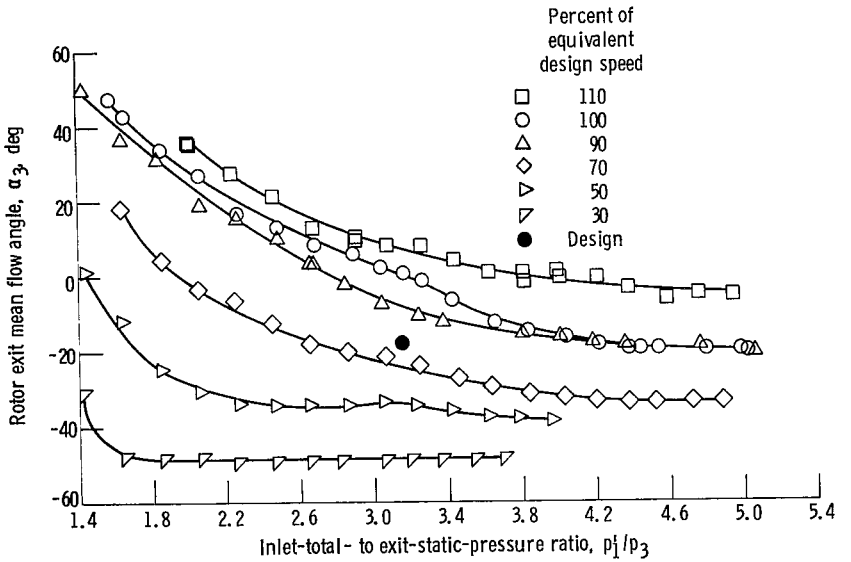

Figure 11. - Variation of rotor exit flow angle with pressure ratio and speed for plugged turbine.

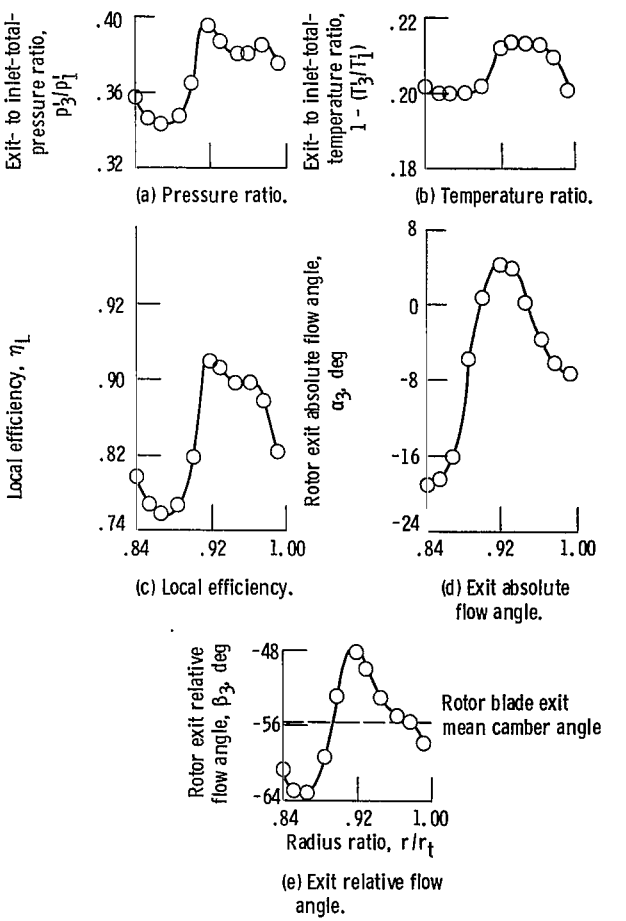

Figure 12. - Variation of pressure ratio, temperature ratio, local efficiency, absolute flow angle for plugged turbine, and relative flow angle with radius ratio at design speed and near design pressure ratio.

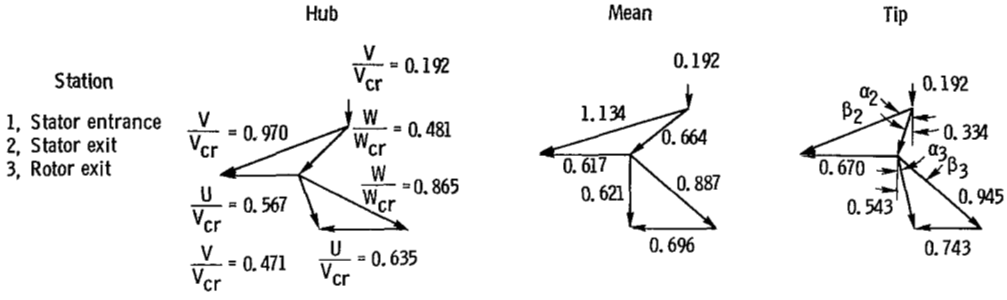

Radius (cm) at -			
Station 1	5.35	5.82	6.31
Station 2	5.35	5.82	6.31
Station 3	5.35	5.82	6.31
α_2, deg	74.4	66.6	70.4
β_2, deg	54.5	43.3	25.9
α_3, deg	-19.2	.1	-11.2
β_3, deg	-60.6	-48.2	-58.1

Figure 13. - Velocity diagrams as calculated from experimental results for plugged turbine.

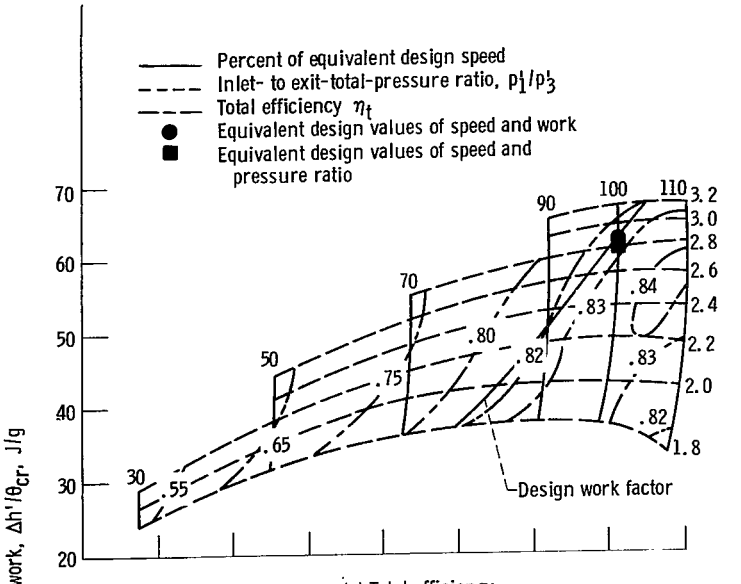

(a) Total efficiency.

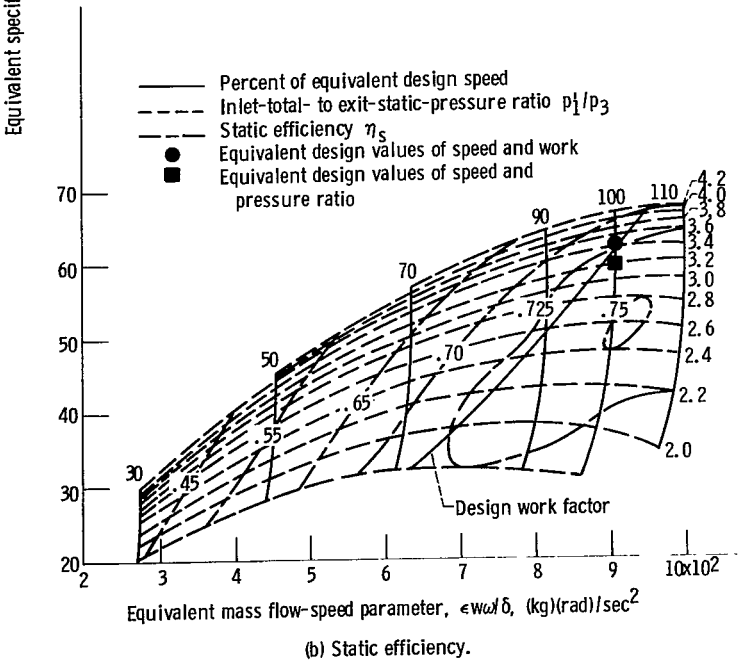

(b) Static efficiency.

Figure 14. - Overall total performance map for plugged turbine.

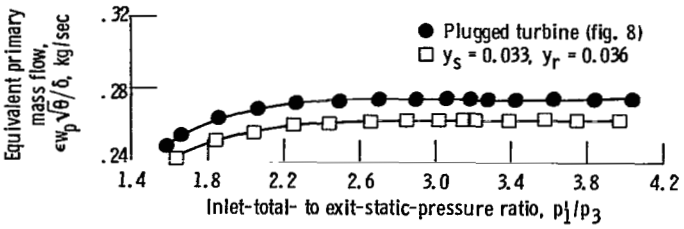

Figure 15. - Variation of mass flow with pressure ratio at 100 percent equivalent design speed.

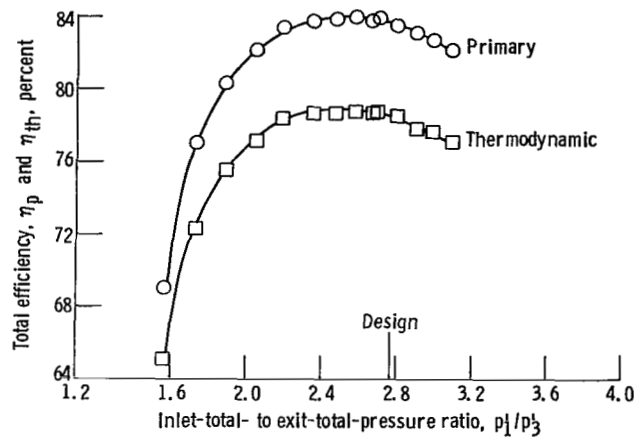

Figure 16. - Variation of primary and thermodynamic efficiency with pressure ratio. Data at 100 percent equivalent design speed with y_s of 0.033 and y_r of 0.036.

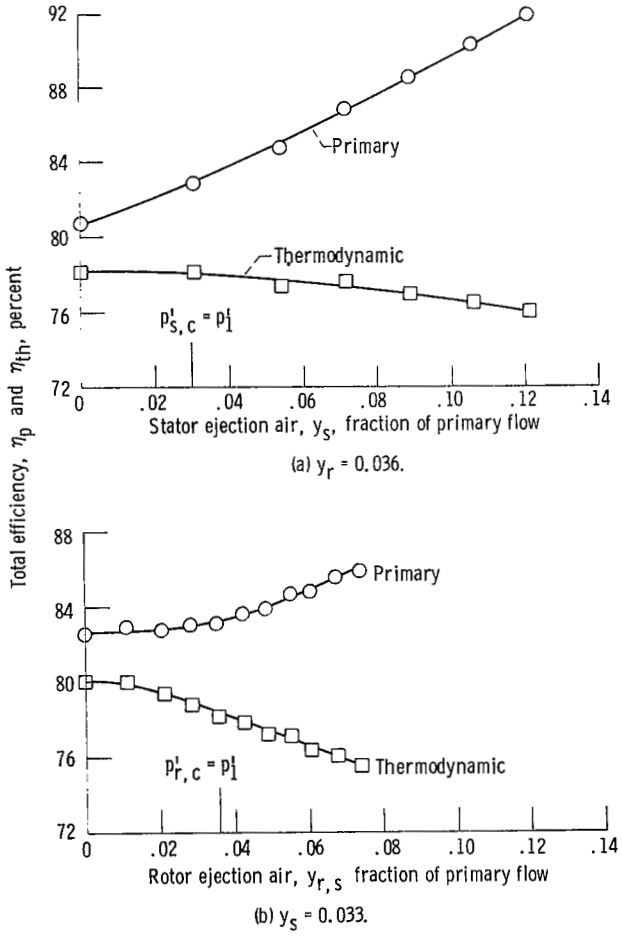

Figure 17. - Variation of primary and thermodynamic efficiency with ejection air. Data at 100 percent equivalent design speed and design total pressure ratio.

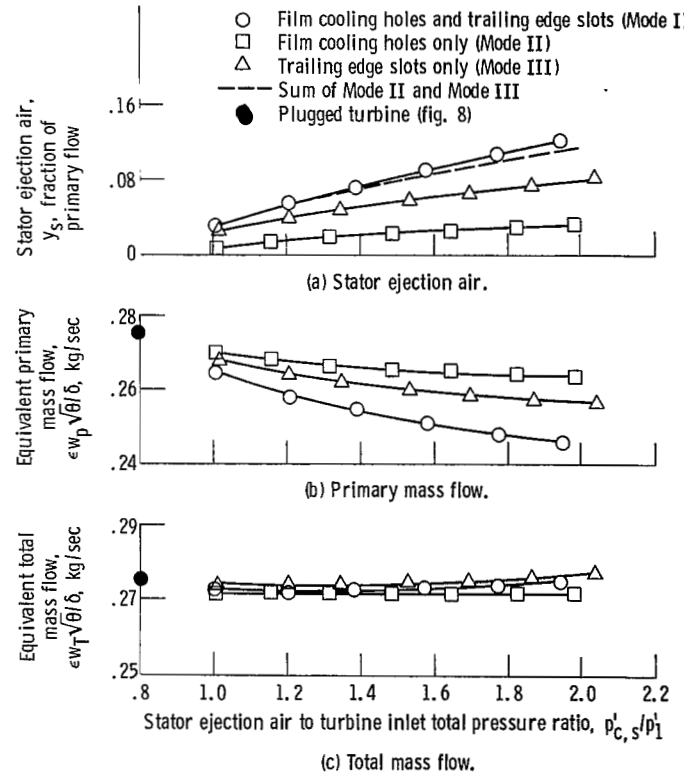

Figure 18. - Variation of stator ejection air, equivalent primary flow and equivalent total flow with stator ejection air total pressure for three modes of film cooling ejection and trailing edge ejection. Data at 100 percent equivalent design speed and design total pressure ratio.

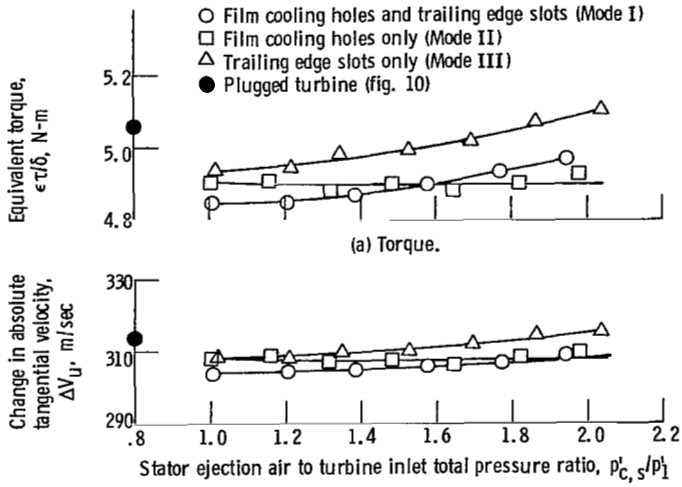

(a) Torque.

(b) Change in absolute tangential velocity.

Figure 19. - Variation of equivalent torque and absolute tangential velocity with stator ejection air total pressure for three modes of film cooling ejection and trailing edge ejection. Data of 100 percent equivalent design speed and design total pressure ratio.

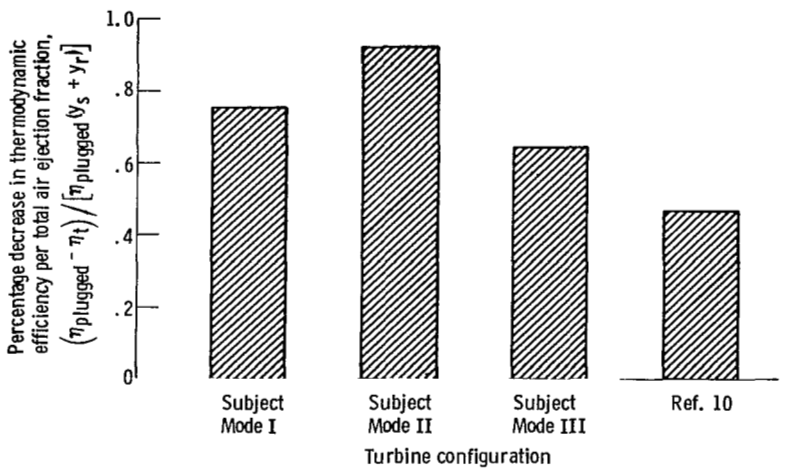

Figure 20. - Comparison of percentage decreases in thermodynamic efficiency between subject turbine and turbine of reference 10.

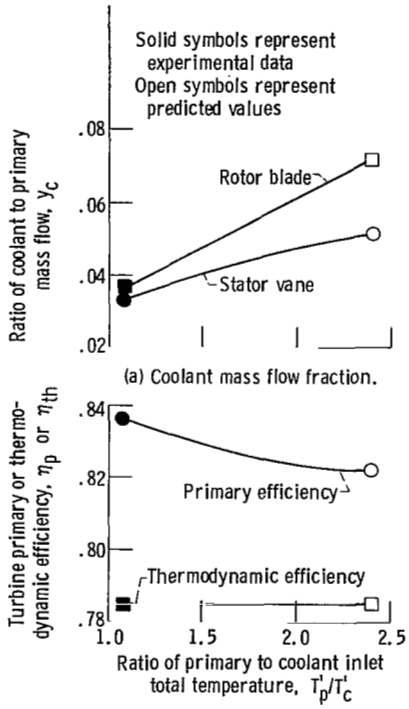

(a) Coolant mass flow fraction.

(b) Turbine efficiency.

Figure 21. - Prediction of coolant mass flow fractions and turbine efficiency at primary to coolant temperature ratio of 2.4 from experimental results and at temperature ratio of 1.08.

1. Report No.	2. Government Accession No.	3. Recipient's Catalog No.
NASA TP-1018		

4. Title and Subtitle: COLD-AIR PERFORMANCE OF A 12.766-CENTIMETER-TIP-DIAMETER AXIAL-FLOW COOLED TURBINE II - EFFECT OF AIR EJECTION ON TURBINE PERFORMANCE

5. Report Date: August 1977

6. Performing Organization Code:

7. Author(s): Jeffrey E. Haas and Milton G. Kofskey

8. Performing Organization Report No.: E-9145

9. Performing Organization Name and Address:
NASA Lewis Research Center and
U.S. Army Air Mobility R&D Laboratory
Cleveland, Ohio 44135

10. Work Unit No.: 505-04

11. Contract or Grant No.:

12. Sponsoring Agency Name and Address:
National Aeronautics and Space Administration
Washington, D.C. 20546

13. Type of Report and Period Covered: Technical Paper

14. Sponsoring Agency Code:

15. Supplementary Notes:

16. Abstract

An air cooled version of a single-stage, axial-flow turbine was investigated to determine aerodynamic performance with and without air ejection from the stator and rotor blade surfaces to simulate the effect of cooling air discharge. Air ejection rate was varied from 0 to 10 percent of turbine mass flow for both the stator and the rotor. A primary-to-air ejection temperature ratio of about 1 was maintained.

17. Key Words (Suggested by Author(s))	18. Distribution Statement
Axial-flow turbine; Single-stage turbine; Gas turbine; Efficiency; Performance tests; Turbine cooling; Blade cooling	Unclassified - unlimited STAR Category 02

19. Security Classif. (of this report)	20. Security Classif. (of this page)	21. No. of Pages	22. Price*
Unclassified	Unclassified	36	A03

* For sale by the National Technical Information Service, Springfield, Virginia 22161